Ballistic- and quantum-conductor carbon nanotubes: The limits of the liquid-metal contact method

M. Kobylko

Laboratoire de Physique des Solides (LPS), CNRS/Université Paris-Sud UMR 8502, Bâtiment 510, Orsay, France
and Laboratoire des Solides Irradiés (LSI), CEA/CNRS/Ecole Polytechnique UMR 7642, Ecole Polytechnique, Palaiseau, France

(Received 13 March 2014; revised manuscript received 31 August 2014; published 20 November 2014)

The liquid-metal contact method (LMC method), which consists of immersing a carbon nanotube (CNT) placed on the apex of a metallic tip into a drop of liquid mercury (Hg), has been previously employed to show ballistic and quantum conductance properties of different kinds of CNTs. Using numerical simulations based on an analytical model of the mechanical interaction between the CNTs and the Hg surface, we show that the LMC method is unsuited for the analysis of ballistic conductance because most CNTs under realistic experimental conditions will not create a mobile contact this way. Furthermore, we show that the apparent electronic mean free path value deduced from these experiments will be exclusively due to elasticity induced CNT bending, geometry induced CNT sliding, and contact angle induced Hg meniscus related effects, and not to the electronic properties of the CNTs. These findings have strong consequences for the interpretation of previously reported works.

DOI: 10.1103/PhysRevB.90.195432 PACS number(s): 73.63.Fg, 61.25.Mv, 73.23.Ad

I. INTRODUCTION

The electronic properties of carbon nanotubes (CNTs, discovered by Iijima [1]) are fascinating. Depending on their diameter and helicity, CNTs can be conductors or semiconductors with different band gaps [2]. These properties make them a promising candidate for becoming the building blocks of a new electronics at the nanoscale [3]. Unfortunately, the question of whether multiwall CNTs (MWNTs) are ballistic [4,5] or diffusive conductors [6,7] has never been satisfactorily resolved, the difficulty of performing length-dependent conductivity measurements on well-characterized CNTs while limiting the influence of the environment (e.g., from the substrate) being one of the main problems.

This experimental challenge seemed overcome with the well-known experiment of Frank *et al.* [4] who reported on two main results. First, they showed that MWNTs behave as ballistic conductors at room temperature and that their electronic mean free paths (EMFPs) amount to several micrometers. Second, they showed that the conductance of MWNTs is quantified and that the quantification step amounts to $G = 1G_0 = 2e^2/h$ [whereas theory [2] predicts $G = 2G_0$ for single-wall CNTs (SWNTs)]. An elegant liquid-metal contact method (LMC method) has been used in this experiment. The goal of this method is to create a mobile electrical contact on a MWNT in order to measure its conductance versus length dependence. The LMC method supposes that this can be achieved by placing MWNTs on the apex of an electrically conductive tip and by immersing them into a liquid metal [generally mercury (Hg); see Fig. 1]. However, even if the LMC method has become widespread experimentally [5,8–12] (see our previous paper [13] for more details), no theoretical study of the physics of CNT-Hg immersion supporting the validity of this macroscopically inspired approach at nanometric length scales has ever been performed.

In our previous paper [13], we have already provided experimental evidence that (i) the *in situ* LMC method (i.e., the LMC method performed within a TEM (transmission electron microscope) which provides real-time visualization of the experiment) is well suited to create low-resistance contacts with CNTs in the nonimmersion configuration depicted in Fig. 1(a) and that (ii) the ballistic and quantum conductance measured by the *ex situ* LMC method (i.e., the LMC method performed without real-time visualization of the experiment) is likely to give false positives in the two configurations (a) and (b) depicted in Fig. 1 for three reasons: (i) the CNTs are likely to be removed from the tip surface through contact with the Hg, (ii) occurring Hg-tip surface nanocontacts are likely to be mistaken for quantum conductor CNTs, and (iii) occurring Hg nanomenisci are likely to be mistaken for ballistic conductor CNTs. However, the question remains of whether ballistic and quantum conductance can be measured with the LMC method in the immersion configuration depicted in Fig. 1(b) in a specially designed *in situ* experiment in which one can ascertain that the electrical measurement is indeed performed on the CNT.

Using numerical simulations based on an analytical model of the mechanical interaction between the CNTs and the Hg surface, we show in this paper that the LMC method is unsuited for the analysis of ballistic conductance because most CNTs under realistic experimental conditions will not create a mobile contact with the Hg in this kind of experiment. In consequence, the so deduced electronic mean free path (EMFP) value will be exclusively due to elasticity induced CNT bending, geometry induced CNT sliding, and contact angle induced Hg meniscus related effects, and not to the electronic properties of the CNTs. These findings have strong consequences for the interpretation of previously reported works.

This paper is organized as follows: After the central quantity of the model (the "supplementary approach distance" l_{sup}) is introduced in Sec. II, some comments on the analytical model of the mechanical CNT/Hg-surface interaction are given in Sec. III. Then, the choice of the presentation modes of the calculation results is described in Sec. IV. This is followed by a description of the practical realization of the calculation in Sec. V. Finally, Sec. VI presents the calculation results and discusses them. The paper closes with a conclusion in Sec. VII.

II. SUPPLEMENTARY APPROACH DISTANCE

In what follows, we will see that a mobile contact on the CNT can be created in two ways: either by the CNT penetrating

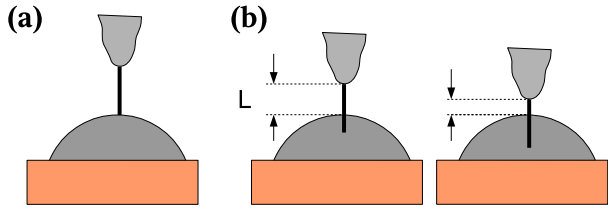

FIG. 1. (Color online) Illustration of the liquid-metal contact (LMC) method: schematic drawing of a CNT placed on a metallic tip being immersed into a drop of liquid metal. In (a), the resistance of the whole CNT is measured, whereas in (b) only the resistance of the nonimmersed part of the CNT is measured. See text for more explanations.

the Hg surface or by the CNT lying down on the Hg surface. In both cases though, the consequences will be the same: From the moment at which the tip of the CNT touches the Hg surface until the moment at which the tip of the CNT moves under the Hg surface or lies down on it, the CNT-carrying sample will have to be approached by a certain distance to the Hg surface which we name the "supplementary approach distance" (l_{sup}). This distance will be a systematic error on the electronic mean-free path (EMFP) of the CNTs one tries to determine by these experiments.

In Sec. VI, we will present the results of these simulations showing that this distance can be of the same order as the EMFPs measured with the liquid-metal contact method. Due to this fact, the liquid-metal contact method does not allow the interpretation of the conductance vs sample displacement measurements in terms of CNT conductance vs CNT length dependence. Therefore, wherever approximations will be necessary for the modeling of mechanical interaction between the CNT and the Hg surface, we will take the liberty to use approximations which underestimate the supplementary approach distance (i.e., underestimate the error of the liquid-metal contact method), even to a large extent, and we will be very careful with approximations which could overestimate the supplementary approach distance (i.e., overestimate the error of the liquid-metal contact method). Section VI will show that even a largely underestimated supplementary approach distance is still so big that it causes the liquid-metal contact method to be unsuitable for the interpretation of the conductance vs sample displacement measurements in terms of CNT conductance vs CNT length dependence. In other words, despite many approximations we make in favor of the LMC method within our model, our model still shows the failure of the LMC method for the kinds of CNTs on which it has been applied and reported in the literature.

III. COMMENTS ON THE ANALYTIC MODEL

This section gives some brief comments on the model which we have developed in order to simulate the mechanical CNT/Hg-surface interaction. A detailed description, describing the whole analytical deduction of this model as well as its underlying physical concepts and their discussion in the framework of this model, is given in the Supplemental Material [14].

This section is organized as follows: First, Sec. III A describes the basic assumptions on which the analytical model is based. Then, Sec. III B illustrates the two possible scenarios which can occur if a CNT approaches a Hg surface: the CNT either penetrates the Hg surface or lies down on it. Finally, Sec. III C briefly comments on the used approximations.

A. Basic assumptions

The model we developed is a classical self-consistent model which takes into account the radius, length, and number of walls of the CNT and the misalignments of the CNT and the Hg surface (described by three angles in space). If we define the sample displacement direction as vertical, the misalignment angle of the CNT (β) is the angle by which it is tilted against the vertical position. The misalignment angle of the Hg surface (φ) is the angle by which it is inclined against the horizontal position. The third misalignment angle (τ) is the angle between the direction in which the CNT is tilted and the direction in which the Hg surface is inclined. These three angles (β, φ, and τ) are visualized in Fig. 2 (see Supplemental Material [14] for more details). Taking these misalignments into account is essential because they cannot be controlled neither in *ex situ* nor in *in situ* experiments.

We assume that, depending on the flexibility of the CNTs, a mobile contact can be created in two ways: either by progressive penetration of the Hg surface by a *rigid CNT* or by progressive lying down of a *flexible CNT* on the Hg surface. This is based on our assumption that the CNT bends like a classical elastic medium (with little modifications) and that the Hg surface acts like a macroscopic Hg surface (with little modifications). Further details and the validity of these approximations are commented on in Sec. III C.

B. Illustration of the possible scenarios

In this model, we divide the CNTs into two categories: If the CNT is sufficiently rigid for the penetration of the Hg surface, we will call it a "rigid CNT." If this is not the case, we will call it a "flexible CNT." Whether a CNT is classified "rigid" or "flexible" does not only depend on the intrinsic properties of the CNT itself (length, radius, number of walls) but also on the three misalignment angles of the CNT and the Hg surface. Note that this classification is without loss of generality because every possible CNT falls in one of these two categories.

In the case of a sufficiently rigid CNT for the penetration of the Hg surface, which can only be a thick short and little misaligned CNT with many walls, the mobile contact is created if the length of the CNT segment having penetrated the Hg surface can be controlled. We assumed that when a rigid CNT approaches the Hg surface beyond the point at which the tip of the CNT touches the Hg surface, the Hg surface will follow the CNT until the contact angle between the CNT and the Hg reaches its equilibrium value. This creates an inverse (concave) meniscus in the Hg surface which takes a shape which, under the given boundary conditions, minimizes its surface. (These liquid-mechanics-related assumptions and their applicability in the present case are based on the works of de Gennes *et al.* [15], Awasthi *et al.* [16], Chen *et al.* [12], Dujardin

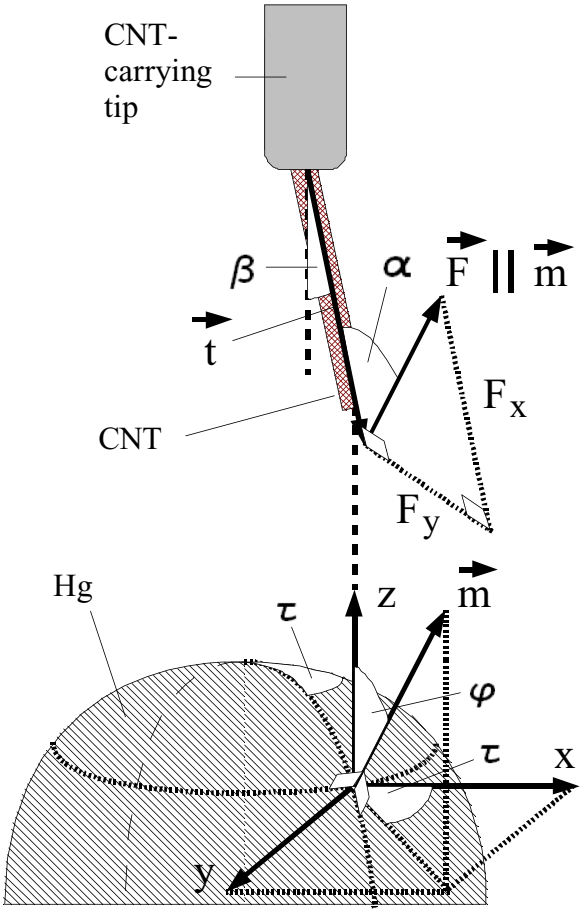

FIG. 2. (Color online) A CNT-carrying tip with a CNT at its apex approaching a Hg droplet. The CNT is entirely contained in the xz plane. Note that the origin of the coordinate system is placed on the point in which the CNT will touch the Hg surface if the CNT carrying approaches sufficiently. $\vec{F} \parallel \vec{m}$, $\vec{F}_x \parallel \vec{t}$, $\vec{F}_y \perp \vec{t}$. $\vec{F}_y$ lies always in the $\vec{t}$-$\vec{m}$ plane but, in the general case, does not lie in the xy plane. See text and the Supplemental Material [14] for the definition of the other quantities.

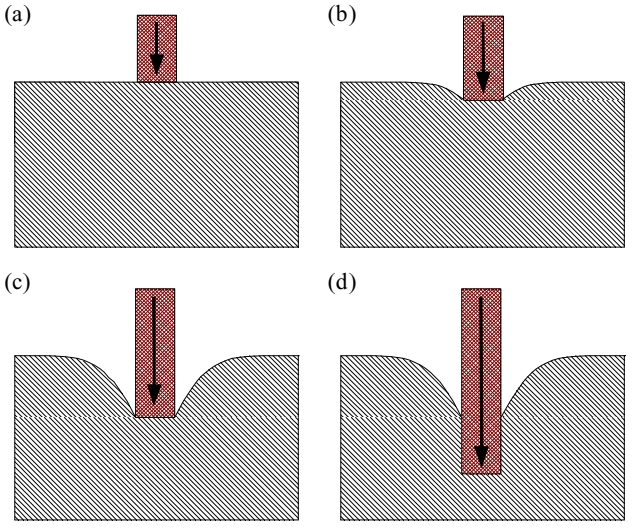

FIG. 3. (Color online) A very rigid CNT, aligned with the direction of the sample displacement, trying to penetrate the Hg surface: (a) at mechanical contact with the Hg surface; (b) pushing the Hg surface and forming and deepening a concave meniscus; (c) the contact angle between the CNT surface and the Hg surface reaches the equilibrium value, $l_{\text{sample}} = l_{\text{sup}}$ (see Fig. 6); (d) the meniscus cannot be deepened any more, so the CNT penetrates the Hg surface. For simplicity, the Hg surface is assumed to be horizontal.

et al. [17,18], Israelachvili *et al.* [19], Tolman [20–22], van Giessen *et al.* [23], Lei *et al.* [24], Schiff [25], Samsonov *et al.* [26], and Lu *et al.* [27]. This subject is explained and justified in more detail in the Supplemental Material [14] in Sec. II.) In order to create and deepen this meniscus, one has to perform work against a force coming from the surface tension of the Hg acting at the circumference of the CNT with a meniscus-depth-dependent contact angle. We assumed that, under this force, the (misaligned) CNT will bend like a classical elastic medium. (These solid-mechanics-related assumptions and their applicability in the present case are based on the works of Yakobson *et al.* [28], Lu *et al.* [29], Hernandez *et al.* [30], Enomoto *et al.* [31], and Poncharal *et al.* [32], using also the textbook of Szabo [33] and the review paper of Grobert [34]. This subject is explained and justified in more detail in the Supplemental Material [14] in Sec. III.) Consequently, the CNT will shorten in the vertical direction and slide on the Hg surface. (The detailed calculations of these effects in the geometry of a LMC experiment are presented in the Supplemental Material [14] in Sec. IV.) All these three effects, the depth of the concave Hg meniscus, the shortening of the CNT, and the sliding of the CNT on the inclined Hg surface, will delay the penetration of the Hg surface by the rigid CNT. (An overview of the calculation steps is presented in the Supplemental Material [14] in Sec. V. An overview and a discussion of the used approximations is presented in the Supplemental Material [14] in Sec. VI.)

For illustration, the penetration mechanism of a very rigid CNT (i.e., a CNT which does not bend noticeably), aligned with the direction of the sample displacement, is shown in Fig. 3. The supplementary approach distance l_{sup} is in this case only caused by the meniscus depth. However, this meniscus depth can be greatly reduced in the case of a very tilted entry of the very rigid CNT, as illustrated in Fig. 4.

If the CNT approaching the Hg surface is not a thick short and little misaligned CNT with many walls, it is more likely that it will rather lie down on the Hg surface than penetrate it. In this case of a "flexible CNT," a mobile contact is created if the length of the CNT segment lying flatly on the Hg surface can be controlled. When a flexible CNT lies down on the Hg surface, only a negligibly small meniscus will be created in the Hg surface which will be sufficient to bend the CNT until its end lies down on the Hg surface. Even if in this situation there is no noteworthy Hg meniscus depth to be taken into account, still the vertical shortening of the CNT and the sliding of the CNT on the inclined Hg surface will delay the lying down of the CNT on the Hg surface.

For illustration, the lying down mechanism of a flexible CNT is shown in Fig. 5. The supplementary approach distance l_{sup} is only caused by the vertical shortening in the illustrated case. If the Hg surface were inclined, which is usually the

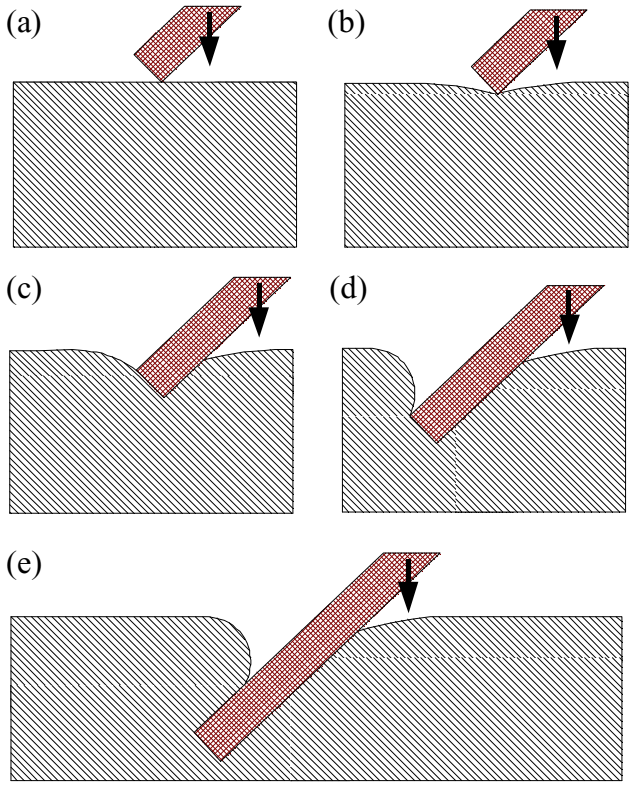

FIG. 4. (Color online) A very rigid CNT, very tilted in respect to the direction of the sample displacement, trying to penetrate the Hg surface: (a) at mechanical contact with the Hg surface; (b) pushing the Hg surface and forming and deepening a concave meniscus; on the right side: the contact angle between the CNT surface and the Hg surface has reached the equilibrium value, $l_{\text{sample}} = l_{\text{sup}}$ (see Fig. 6); (c) on the left side: deepening the concave meniscus; on the right side: the meniscus cannot be deepened any more, so the CNT penetrates the Hg surface; (d) on the left side: the contact angle between the CNT surface and the Hg surface reaches the equilibrium value; (d) the meniscus on the left side cannot be deepened any more, so the CNT also penetrates the Hg surface on the left side. For simplicity, the Hg surface is assumed to be horizontal.

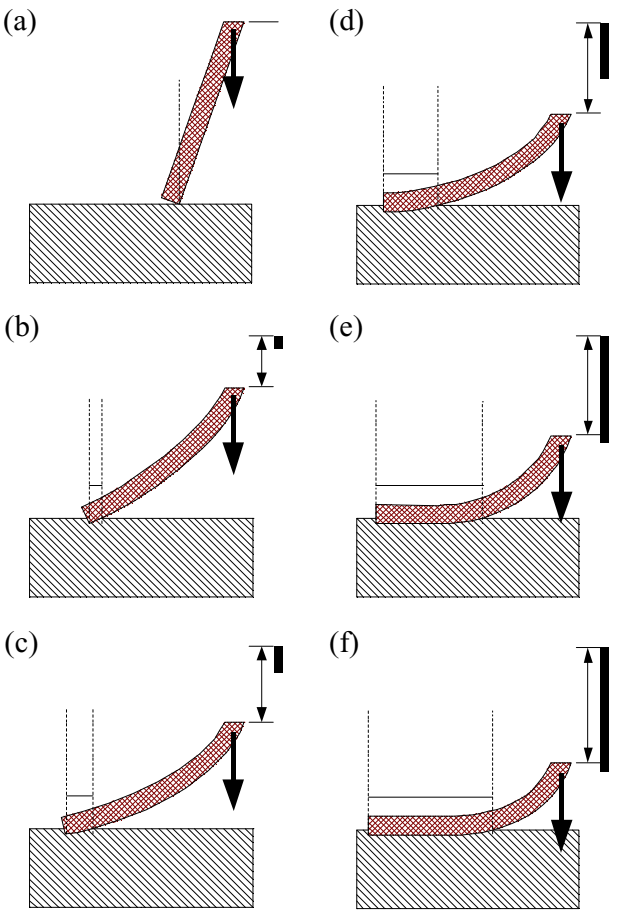

FIG. 5. (Color online) A flexible CNT trying to intrude into the Hg surface but instead lying down on it. For simplicity, the Hg meniscus is not shown. Shown is the sample displacement (vertical double arrow) and the length of the contacted CNT wall (horizontal line and bold vertical line) which, however, is not accurate. The CNT is (a) at mechanical contact with the Hg surface; (b) and (c) bending and sliding on the Hg surface; (d) unable to bend any further as its end has lain down on the Hg surface; (e) and (f) progressively lying down on the Hg surface. For simplicity, the Hg surface is assumed to be horizontal.

case, sliding of the CNT end on the Hg surface would also contribute to l_{sup}.

It may be helpful to illustrate the length of the Hg-contacted CNT wall l_{contact} vs the sample displacement l_{sample} dependence. Figure 6 shows this dependence for an aligned/tilted rigid/flexible CNT. The differences between different kinds of CNTs can be summarized as follows: The difference between an aligned and a tilted CNT (both rigid or flexible) is that for an aligned CNT, l_{contact} is always smaller than l_{sample}, while for a tilted CNT, l_{contact} can become bigger than l_{sample} when l_{sample} becomes as big as several l_{sup}. The difference between a rigid and a flexible CNT (both aligned or tilted) is that for a rigid CNT, l_{contact} is always equal to zero when $l_{\text{sample}} < l_{\text{sup}}$, while for a flexible CNT, l_{contact} is bigger than zero (but considerably smaller than l_{sup}) when $l_{\text{sample}} < l_{\text{sup}}$. In all cases, one sees that the l_{contact} vs l_{sample} dependence differs significantly from the usually assumed $l_{\text{contact}} = l_{\text{sample}}$ relationship. Only for $l_{\text{sample}} > l_{\text{sup}}$, one can expect an approximately linear relationship between l_{contact} and l_{sample} but never $l_{\text{contact}} = l_{\text{sample}}$.

C. Comments on the used approximations

This section presents a brief summary of the discussion of the used approximations. A more detailed discussion and overview of the used approximations can be found in the Supplemental Material [14] in Sec. VI.

The approximations used in this model can be divided in three categories: (a) approximations overestimating the supplementary approach distance, (b) approximations overestimating or underestimating the supplementary approach distance, and (c) approximations underestimating the supplementary approach distance. We have avoided approximations of the first and second kind whenever possible and have used approximations of the third kind where reasonable.

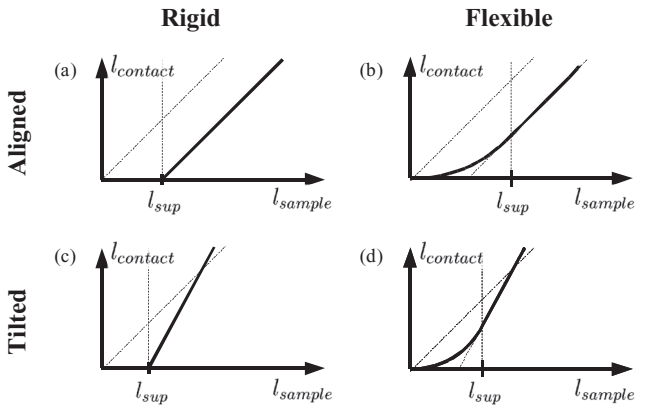

FIG. 6. Length of the Hg-contacted CNT wall l_{contact} vs the sample displacement l_{sample} for (a) an aligned rigid CNT, (b) an aligned flexible CNT, (c) a tilted rigid CNT, and (d) a tilted flexible CNT. The supplementary approach distance l_{sup} is defined as the l_{sample} at which respectively the end of the rigid CNT penetrates the Hg surface or the end of the flexible CNT lies down on the Hg surface. These graphs are not to scale in respect to each other and those concerning the flexible CNT are not calculated but just very roughly estimated using oversimplified assumptions. (Note that l_{contact} of a flexible CNT cannot be calculated in the framework of this model. Only l_{sup} of a flexible CNT can be calculated in the framework of this model and is the only quantity that needs to be calculated for our purpose.) In particular, the l_{contact} vs l_{sample} relationship for a flexible CNT is not necessarily linear for $l_{\text{sample}} > l_{\text{sup}}$ even if this is shown this way in (b) and (d). For comparison, the usually assumed $l_{\text{contact}} = l_{\text{sample}}$ relationship is indicated as a dashed line. For simplicity, the Hg surface is assumed to be horizontal.

As a reminder, underestimating the supplementary approach distance l_{sup} is equivalent to overestimating the mobile contact creation probability (which is in favor of the LMC method and therefore in agreement with the goal of this model, defined in Sec. II).

The following estimations of the accuracy of the used approximations are only as accurate as necessary to ascertain that the goal of this model, i.e., an effective total underestimation of l_{sup} rather than an overestimation, has been met. They are not only based on the analytical framework presented in the Supplemental Material [14] but also on the usual numerical data for the CNT distributions which we have studied numerically.

The first category of approximations (those which might overestimate the supplementary approach distance) contains two approximations: First, at nanoscale the Hg surface tension will probably decrease slightly and the Hg-CNT contact angle might increase or decrease slightly. Consequently, using the macroscopic Hg surface tension value and the macroscopic Hg-graphite contact angle value might overestimate l_{sup} roughly by a factor of 2 (see Sec. IV of the Supplemental Material [14] for details). Second, the possibility of the Hg slightly climbing up the CNT wall (if the free CNT end is nearly parallel to the Hg surface) is neglected. Consequently, this approximation might overestimate l_{sup} by very roughly 5% (see Sec. IV of the Supplemental Material [14] for details).

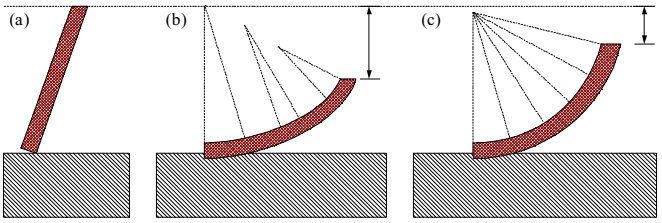

FIG. 7. (Color online) Illustration of the shortening of a CNT through bending. Shown is a flexible CNT lying down on the Hg surface. For simplicity, the Hg meniscus is not shown. The vertical double arrow shows the sample displacement (the drawing is not accurate) which corresponds to the bending-induced part of the supplementary approach distance l_{sup}. The CNT is (a) at mechanical contact with the Hg, (b) bent with a high curvature close to the CNT-carrying tip and with a low curvature close to the Hg surface (more accurate model), and (c) bent with a constant curvature (simple approximation used for this model).

The second category of approximations (those which might overestimate or underestimate the supplementary approach distance) also contains two approximations: First, the fact that the maximal radial extension of the Hg meniscus can only be badly defined might over- or underestimate l_{sup} by very roughly 5% (see Sec. IV of the Supplemental Material [14] for details). Second, the calculation of the perpendicular bending deviation of the CNT with a formula which is only exact for small bending deviations might over- or underestimate l_{sup} by roughly 33% in the worst case (see Sec. IV of the Supplemental Material [14] for details).

Finally, the third category of approximations (those which underestimate the supplementary approach distance) contains three approximations: First, the intentional underestimation of the repulsive force of the Hg surface in the case of a tilted intrusion of the CNT underestimates the supplementary approach distance l_{sup} very roughly by a factor of 2 (see Sec. IV of the Supplemental Material [14] for details). Second, the intentional overestimation of the Young modulus of CNTs underestimates the supplementary approach distance l_{sup} very roughly at least by a factor of 5 (see Sec. IV of the Supplemental Material [14] for details). Third, we have not calculated the shortening of the total longitudinal extension of the CNT through its bending in a detailed model but in a constant-curvature approximation. This approximation usually underestimates the supplementary approach distance l_{sup} very roughly by a factor of at least 1.5 (see Fig. 7 and Sec. IV of the Supplemental Material [14] for details).

Therefore, we can conclude that our model presented in this paper underestimates the supplementary approach distance by a factor of between 5 and 10 (see Sec. IV of the Supplemental Material [14] for details). This means that it overestimates the mobile contact creation probability noticeably. Hence, should the mobile contact creation probability values calculated with this model be too low for the liquid-metal contact method to work, they would be even lower when calculated with a more detailed model. In conclusion, the here presented model together with the chosen approximations is suitable for deciding between two possibilities: either (a) that the LMC method might work or (b) that the LMC method fails. In what

follows, we show that numerical simulations based on this model confirm possibility (b).

IV. CHOICE OF THE PRESENTATION MODES OF THE CALCULATION RESULTS

The model we have developed calculates the supplementary approach distance l_{sup} in dependence on six parameters: the radius, the length, and the wall number of the CNT, and the three misalignment angles in space of the CNT and the Hg surface. Indeed, the wall number may be assumed to be known during an *ex situ* transport experiment as it is often approximately constant over an experimental CNT distribution but this still leaves five unknown parameters. In order to show the dependency of l_{sup} on all these parameters one by one, one would need a six-dimensional graph. As this is not feasible, the choice of the proper presentation mode is important. This section presents two possible presentation modes, the supplementary approach distance map (helpful for the visualization of the effect of the CNT length and CNT radius) and the mobile contact creation probability graph (helpful for the interpretation of experimental results).

A. Supplementary approach distance map for an experimental CNT distribution

The supplementary approach distance map (see example in Fig. 8) is particularly adapted to estimate quickly the approximate order of magnitude of l_{sup} of an experimental CNT distribution as well as for visualizing the dependence of l_{sup} on the radius and the length of a CNT. However, such a map is always calculated only for a fixed set of the three misalignment angles of the CNT and the Hg surface. As these angles cannot be controlled in an *ex situ* transport experiment, this map is only useful for interpretation of experimental results if it is shown together with other maps calculated for other sets of misalignment angles.

Figure 8(e) gives the legend for the four maps shown in Figs. 8(a), 8(b), 8(c), and 8(d). Maps 8(a) and 8(c) [showing a zoom of the lower left corner of 8(a)] have to be interpreted with the color code shown in 8(e) where red stands for $l_{sup} = 0.1\ \mu$m *or smaller* and pink stands for $l_{sup} = 1.0\ \mu$m *or bigger*. The most eye-catching feature of these maps is the rainbow-like line going from the lower left corner to the upper right corner of these maps. Indeed, this line can be understood as the separation between the flexible CNTs on the upper left side of the map (long thin CNTs) and the rigid CNTs on the lower right side of the map (short thick CNTs). In both cases, the dependence of l_{sup} on L (vertical axis) and R (horizontal axis) can be understood easily.

The l_{sup} of flexible CNTs arises only from the shortening and sliding of the CNTs through bending. A flexible CNT is always bent to the maximal extent, no matter what its radius is. Therefore, l_{sup} does not vary with R on the upper left side of the map but only with L (the longer the CNT is, the more it bends). Therefore, l_{sup} increases from the bottom to the top on the left side of the map.

In contrast, l_{sup} of rigid CNTs arises not only from the shortening and sliding of the CNTs through bending but also through meniscus creation in the Hg surface. The depth of the meniscus is very roughly proportional to the radius of the CNT. Therefore, we can see an increase of l_{sup} from the left to the right at the bottom of the map. In addition, in contrast to a flexible CNT, a rigid CNT never bends to its maximal extent. Thus, the contribution to l_{sup} arising from shortening and sliding through bending depends on both the length and the radius of the CNT (the thinner and the longer the CNT is, the more it bends). Therefore, one should see l_{sup} increasing from the right to the left and from the bottom to the top on the right lower side of the map. Indeed, one can see this dependency. It is nothing else than the rainbow-like line in the middle of the map.

The reason why this dependency can only be seen in such a small fraction of the map can easily be explained. As shown in the Supplemental Material [14], the rigidity of the CNT depends sensitively on its outer radius ($\propto R^4$) and on its length ($\propto 1/L^2$). As both R and L vary over as much as an order of magnitude, the rigidity of the CNT ($\propto R^4/L^2$) varies over several orders of magnitude. Thus, most of the CNTs are either very rigid, i.e., hardly bend at all, or very flexible. Only a small fraction of a typical experimental distribution has exactly the precise rigidity to make them bend noticeably but not to the maximal extent. Therefore, the rainbow-like line covers only a small fraction of the map and can be understood as the separation line between the rigid and the flexible CNTs.

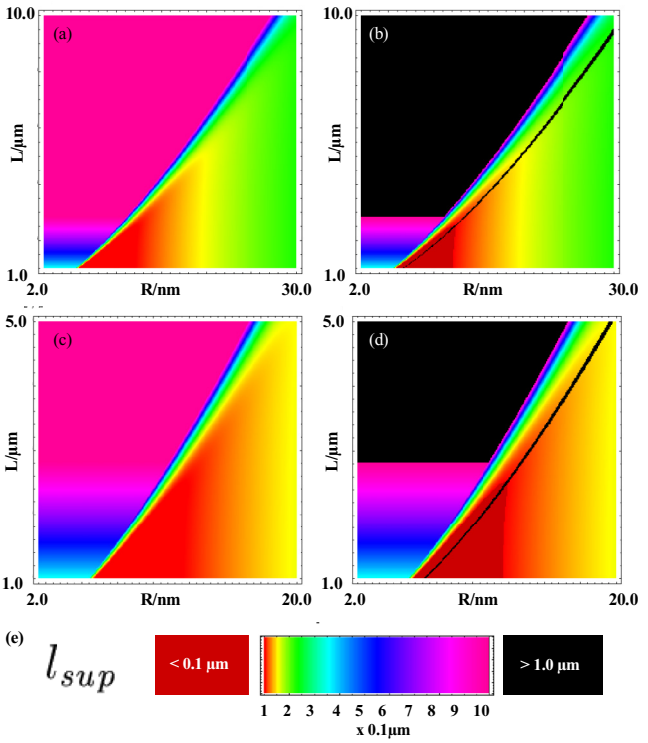

FIG. 8. (Color online) The supplementary approach distance map shows the supplementary approach distance l_{sup} for each combination between the CNT radius R and the CNT length L out of the experimental CNT distribution. However, one needs several maps in order to show the variation of l_{sup} with the three misalignment angles of the CNT and the Hg surface. The parameters are full MWNTs, $E = 5$ TPa, $\beta = 0.001°$, $\varphi = 0.001°$, and $\tau = 89.999°$ in all four maps. See text for explanations.

(Note that these CNTs which are on the rainbow-like line are still rigid CNTs according to the definition used in this paper because, even if they bend noticeably, they do not bend to the maximal extent.)

The maps 8(b) and 8(d) are almost identical to the maps 8(a) and 8(c), except for the fact that they contain three additional pieces of information. First, the region of the map where l_{sup} is smaller than 0.1 μm is no longer coded with red but with brown (see the brown triangle at the bottom of the maps). Second, the region of the map where l_{sup} is bigger than 1.0 μm is no longer coded with pink but with black (see the upper left part of the maps). Third, an additional black line (going from the lower left to the upper right part) has been included in the map. This line separates the lower right part of the map, where the perpendicular deviation of the CNT through bending is still small enough to describe the bending of the CNT by a linear differential equation, from the upper left part of the map, where this is no longer the case. (Note that the precise location of this line depends on the precision limit which we have chosen for this calculation. A more generous precision limit would shift this line to the upper left whereas a more severe precision limit would shift it to the lower right.) This line can be helpful for the estimation of the precision of the calculation results.

The modifications added to the maps in 8(b) and 8(d) make these maps more easily readable: Now, the colored surface corresponds to the CNTs which create a mobile contact with the Hg before the sample displacement l_{sample} reaches the here chosen limit 1 μm, and the black surface corresponds to the CNTs which do not. One can also easily find out if the mobile contact is mainly achieved by lying down on the Hg surface or by the penetration of the Hg surface with the help of the rainbow-like line. This line separates the colored surface into two parts: the flexible CNTs which create a mobile contact with the Hg by lying down on its surface and the rigid CNTs which create a mobile contact with the Hg by penetrating its surface.

For example, map 8(b) tells us that for the here chosen misalignment angles, only about 60% of the here chosen experimental distribution of CNTs would make a mobile contact with the Hg for $l_{\text{sample}} \leqslant 1$ μm. For about 50% of the distribution, the mobile contact would be established by penetration of the Hg surface and for about 10% by lying down on the Hg surface. To give another example, map 8(d) [which shows a subdistribution of map 8(b)] tells us that, for the here chosen misalignment angles, only about 70% of the here chosen experimental distribution of CNTs would make a mobile contact with the Hg for $l_{\text{sample}} \leqslant 1$ μm. For about 50% of the distribution, the mobile contact would be established by penetration of the Hg surface and for about 20% by lying down on the Hg surface.

B. Mobile contact creation probability graph for an experimental CNT distribution

The mobile contact creation probability graph (see example in Fig. 9) is better adapted for the interpretation of experimental results. For a given experimental CNT distribution, it shows the probability of the creation of a mobile contact if, from the moment in which one arbitrarily chosen CNT touches the Hg surface, the CNT-carrying sample is approached by a given distance l_{sample} to the Hg surface. This probability is shown as a function of the maximal misalignment angle of the CNT β_{max} and the maximal inclination angle of the Hg surface φ_{max} which are two parameters which can be estimated for a given set of experiments. (Thus, the mobile contact creation probability graph shows the probability integrated over all possible misalignment angles $0^\circ \leqslant \beta \leqslant \beta_{\text{max}}$ and $0^\circ \leqslant \varphi \leqslant \varphi_{\text{max}}$.) The third misalignment angle τ, i.e., the angle between the direction in which the CNT is tilted and the direction in which the Hg surface is inclined, cannot be controlled and is therefore left free (i.e., we integrate over all possible values $0^\circ \leqslant \tau < 360^\circ$). In order to be able to present the results in a two-dimensional graph, β_{max} is set equal to φ_{max}. (Note that this choice does not affect the fact that $\beta \neq \varphi$ in general. Only β_{max} and φ_{max} are set equal, not β and φ.)

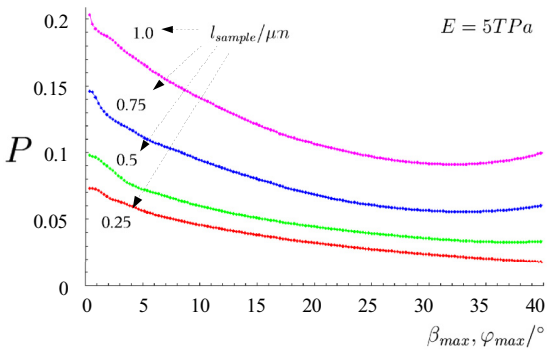

FIG. 9. (Color online) The mobile contact creation probability graph shows the percentage of the CNTs in the given distribution for which the calculated l_{sup} is smaller than the given l_{sample}, and this in dependence of the maximal misalignment angle one can experimentally guarantee for the CNT (β_{max}) and the Hg surface (φ_{max}). The parameters of the experimental distribution are $R = 2.5 \ldots 12.5$ nm and $L = 1.0 \ldots 10.0$ μm. The CNTs are approximated as full tubes (the stiffest CNTs possible). See text for explanations.

Hence, the mobile contact creation probability graph shows the percentage of the CNTs in the given distribution for which the calculated l_{sup} is smaller than the given l_{sample}, and this as a function of the maximal misalignment angle one can experimentally guarantee for the CNT and the Hg surface. In other words, it shows the percentage of the CNTs in the given distribution for which a mobile liquid-metal contact has been created after the sample has been approached by a supplementary distance l_{sample} to the Hg surface. (l_{sample} would be the immersion length of the CNT into the Hg if the CNT were infinitely stiff and aligned and the Hg surface not deforming.) The probabilities for several different l_{sample} can easily be represented in the same graph. In Fig. 9 can be seen that usually the mobile contact creation probability decreases with increasing maximally allowed deviation angle. This is what one would expect in the first place, as a tilted rigid CNT trying to penetrate the Hg surface experiences a higher torque from the latter and therefore bends more than an aligned CNT would do. However, for some l_{sample} one can also state that the probability increases with increasing maximally allowed deviation angle when the latter is approximately $35^\circ \ldots 40^\circ$. This can be explained by the fact that for such high misalignment angles the mobile contact creation is indeed

facilitated for flexible CNTs because, if the constellation of the CNT and the Hg surface is right, a 40° tilted CNT trying to lie down on a 40° inclined surface might need to bend only 10° more in order to create a mobile contact with the Hg surface whereas an aligned CNT has to bend 90° in order to lie down on a noninclined Hg surface.

Figure 9 tells us for example that, for the here chosen experimental CNT distribution and for a typical experimentally achievable maximal misalignment angle of 30°, the probability of mobile contact creation is 2.4% for $l_{\text{sample}} = 0.25\ \mu$m, 3.6% for $l_{\text{sample}} = 0.5\ \mu$m, 5.6% for $l_{\text{sample}} = 0.75\ \mu$m, and 9.1% for $l_{\text{sample}} = 1.0\ \mu$m. With these numbers, one can for example show that even if 9.1% of the CNTs created a mobile contact with the Hg after the sample has been approached by 1.0 μm to the Hg surface, still $9.1\% - 5.6\% = 3.5\%$ would have an error of at least 0.75 μm on the electronic mean free path (EMFP) of the CNT one tries to determine by these experiments. Analogously, $5.6\% - 3.6\% = 2.0\%$ would have an error between 0.5 μm and 0.75 μm on the EMFP, $3.6\% - 2.4\% = 1.2\%$ an error between 0.25 μm and 0.5 μm on the EMFP, and 2.4% an error between 0 and 0.25 μm on the EMFP.

Finally, we want to draw the attention to the following fact: the mobile contact creation probability one could deduct from a l_{sup} map (presented in Sec. IV A) by dividing the colored area through the total area of the map is only a *differential* mobile contact creation probability as it only describes the situation when all three angles have the given precise value. In contrast, the mobile contact creation probability as shown in the here described mobile contact creation probability graph is a *cumulated* mobile contact creation probability which means that it is integrated over all possible angles β and φ below $\beta_{\max}$ and $\varphi_{\max}$ (here, we have set $\beta_{\max} = \varphi_{\max}$) and over all possible angles τ. For these reasons, the mobile contact creation probability graph is the form of presentation which is better adapted for the interpretation of the experimental results. Therefore, in what follows the main conclusions will be drawn from data represented this way.

V. REALIZATION OF THE CALCULATION AND CALCULATION PARAMETERS

This section describes the practical realization of the simulation and the calculation parameters. The calculation code we have developed calculates the mobile contact creation probability graph (see Sec. IV B) for an experimental CNT distribution. For this, a *numerical integration* of the binary condition $l_{\text{sup}} < l_{\text{sample}}$ (i.e., "minimum sample displacement necessary for mobile contact creation" < "performed sample displacement": "True" → 1, "False" → 0) in a *five-dimensional hyperspace* spanned by the CNT radius R, the CNT length L, the CNT misalignment angle β, the Hg surface misalignment angle φ, and the misalignment angle τ between the two planes in which the Hg surface and the CNT are misaligned is necessary. We have implemented this code as a Mathematica [35] procedure and executed it on a standard office PC.

Using the final version of the code, we have performed ten simulations for four different distributions of CNTs (for two distributions assuming three different elastic moduli E for the CNTs and for the other two distributions assuming two different elastic moduli E for the CNTs), corresponding to the parameters of CNTs used by other groups in *ex situ* liquid-metal contact method experiments. All the simulations have been performed for four different sample displacements simultaneously. Usually, one simulation (i.e., the calculation of one mobile contact creation probability graph for one experimental CNT distribution) could take up to 30 hours, i.e., about 10^5 s, and involve the calculation of l_{sup} values for roughly 10^8 (one hundred millions) different CNTs (with about a thousand l_{sup} values calculated per second). These CNT distributions are as follows:

(1) two distributions of MWNTs, corresponding to the CNT parameters published by Frank *et al.* [4], and by Kajiura *et al.* [10];

(2) one distribution of DWNTs, corresponding to the CNT parameters published by Kajiura *et al.* [8];

(3) one distribution of SWNTs, corresponding to the CNT parameters published by Kajiura *et al.* [9].

Table I shows the parameters of these CNT distributions in detail.

With regard to the high dimensionality of this integration process, a proper choice of the integration step, separately for each dimension, is essential in order to ensure both a sufficient precision of the results and a reasonable calculation time. Therefore, each single simulation was preceded by the evaluation of and quest for the best integration steps (see Supplemental Material [14] Sec. VI for details).

TABLE I. Details of the CNT distributions for which we have carried out simulations. Where a "?" appears, these parameters have not been explicitly given in the cited works, and we have made estimations from a figure in Kajiura *et al.* [8] and in Kajiura *et al.* [9] instead, or it corresponds to the most favorable scenario with regard to a rapid penetration of the CNT into the Hg (stiffest CNTs possible) in the case of Frank *et al.* [4] and Kajiura *et al.* [10]. Where the number of walls N_{walls} is preceded by a "∼" (distributions of Frank *et al.* [4] and of Kajiura *et al.* [10]), it is only indicative, and the outer CNT radius R and its inner radius r_i are determinative. In the opposite case when the number of walls N_{walls} is not preceded by a "∼" (distributions of Kajiura *et al.* [8] and Kajiura *et al.* [9]), R and N_{walls} are determinative, r_i not being needed. All simulations have been performed for the following sample displacement l_{sample} values: 0.25 μm, 0.5 μm, 0.75 μm, and 1.0 μm. l_{sample} would be the immersion length of the CNT into the Hg if the CNT were infinitely stiff and aligned and the Hg surface not deforming.

Source	L/μm	R/nm	r_i/nm	N_{walls}	E_Y/TPa
[4]	1 . . . 10	2.5 . . . 12.5	0 ?	∼15	5
[4]	1 . . . 10	2.5 . . . 12.5	0 ?	∼15	1
[4]	1 . . . 10	2.5 . . . 12.5	0 ?	∼15	0.1
[10]	1 . . . 5	5 . . . 10	0 ?	∼15	5
[10]	1 . . . 5	5 . . . 10	0 ?	∼15	1
[10]	1 . . . 5	5 . . . 10	0 ?	∼15	0.1
[8]	4 . . . 5 ?	1 . . . 3.5		2	5
[8]	4 . . . 5 ?	1 . . . 3.5		2	1
[9]	2 . . . 3 ?	0.6 . . . 0.8		1	5
[9]	2 . . . 3 ?	0.6 . . . 0.8		1	1

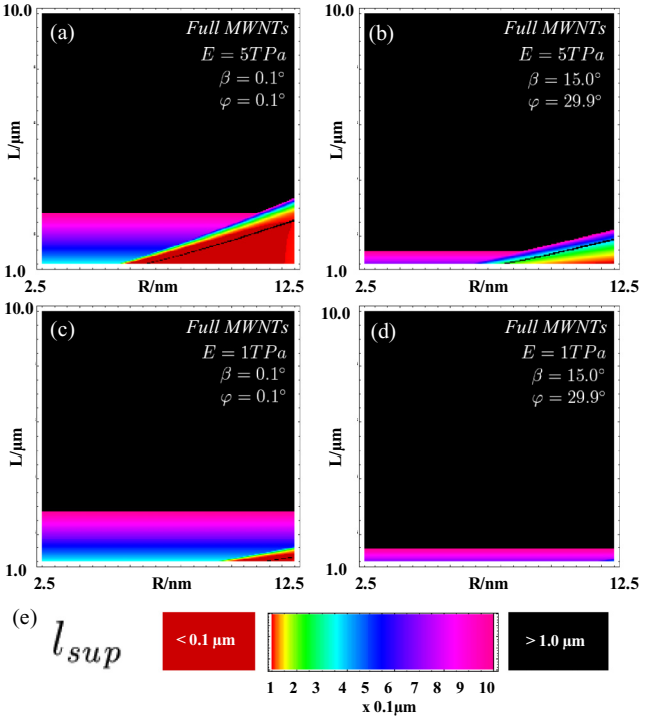

FIG. 10. (Color online) l_{sup} maps for a distribution of full MWNTs (stiffest MWNTs possible) with parameters of Frank *et al.* [4], (a) and (b) for $E = 5$ TPa; (c) and (d) for $E = 1$ TPa. ($\tau = 89.9°$.)

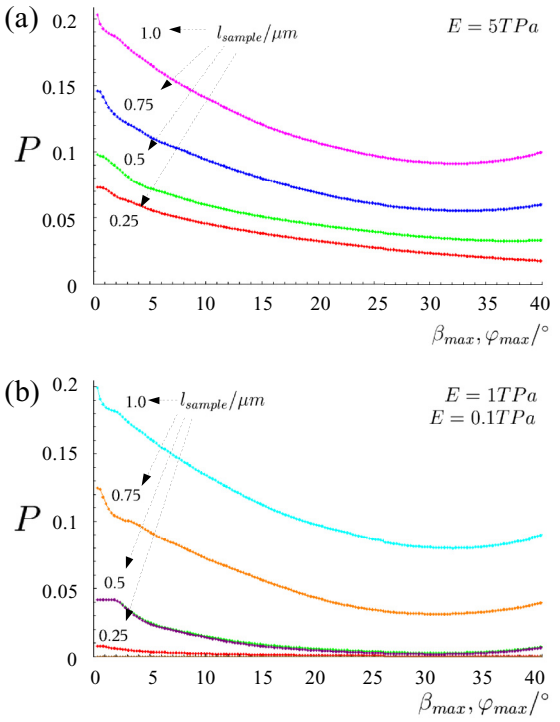

FIG. 11. (Color online) Mobile contact creation probability graphs for a distribution of full MWNTs (stiffest MWNTs possible) with parameters of Frank *et al.* [4], (a) for $E = 5$ TPa; (b) for $E = 1$ TPa and $E = 0.1$ TPa.

VI. CALCULATION RESULTS AND DISCUSSION

In general, the results of our simulations show that whether a CNT will create a mobile contact with the Hg or not depends very much on the precise length, diameter, wall number, and misorientations of the CNT and the Hg surface. Our simulation code integrates the probability over all deviation and inclination angles of the CNT and the Hg surface below a given maximum deviation angle which is meant to correspond to the maximum deviation angle the experimenter can guarantee. In *in situ* experiments this angle will typically be around 30°, and in *ex situ* experiments without visual control this angle can be even as high as 40°. This typical misalignment of the CNTs is for example visualized in Poncharal *et al.* [36], Wang *et al.* [37], Poncharal *et al.* [38], and Berger *et al.* [39]. Usually, if ever a CNT creates a mobile contact with the Hg, it only does so after the sample has approached the Hg surface by a supplementary approach distance l_{sup}. This displacement, from the first electrical contact to the creation of the mobile contact, can be of the order of μm, thus pretending ballistic transport over the CNT on a micrometric length scale. In what follows, we want to present the simulation results for the experimental CNT distributions presented in Sec. V.

For the experimental distribution of MWNTs of Frank *et al.* [4], the results are shown in Figs. 10, 11, and 12. Figure 10 shows some example l_{sup} maps for this distribution. We can make several observations on these figures. First, we can see that the differential mobile contact creation probability does not exceed about 20% for the small-angle limit [see Figs. 10(a) and 10(c)]. It even decreases to 5% for midsize angles [see Figs. 10(b) and 10(d)]. Second, we see that for a Young modulus $E = 5$ TPa [see Figs. 10(a) and 10(b)] very roughly about half of the CNTs creating a mobile contact are rigid CNTs which create the mobile contact by penetration of the Hg surface. However, if we assume a Young modulus $E = 1$ TPa [see Figs. 10(c) and 10(d)], the fraction of these rigid CNTs almost drops to zero. The total differential mobile creation probability (for $l_{\text{sample}} = 1$ μm) however does not differ much between $E = 5$ TPa and $E = 1$ TPa as the decrease of the number of rigid CNTs making a mobile contact with the Hg is nearly compensated by a rise of the number of flexible CNTs making a mobile contact with the Hg.

Turning our attention now to Fig. 11(a), we can see that for a typical experimentally achievable maximal misalignment angle of 30°, the probability of mobile contact creation is 2.4% for $l_{\text{sample}} = 0.25$ μm, 3.6% for $l_{\text{sample}} = 0.5$ μm, 5.6% for $l_{\text{sample}} = 0.75$ μm, and 9.1% for $l_{\text{sample}} = 1.0$ μm. We can conclude from these numbers that even if 9.1% of the CNTs created a mobile contact with the Hg after the sample has approached the Hg surface by 1.0 μm, still $9.1\% - 5.6\% = 3.5\%$ would have an error of at least 0.75 μm on the electronic mean free path (EMFP) of the CNT one tries to determine by these experiments. Analogously, $5.6\% - 3.6\% = 2.0\%$ would have an error between 0.5 μm and 0.75 μm on the EMFP, $3.6\% - 2.4\% = 1.2\%$ an error between 0.25 μm and 0.5 μm on the EMFP, and 2.4% an error between 0 μm and 0.25 μm on the EMFP. Given the high proportion of flexible CNTs making a mobile contact with the Hg, these mobile contact creation probability values are very likely still noticeably overestimated. Therefore, transport experiments performed

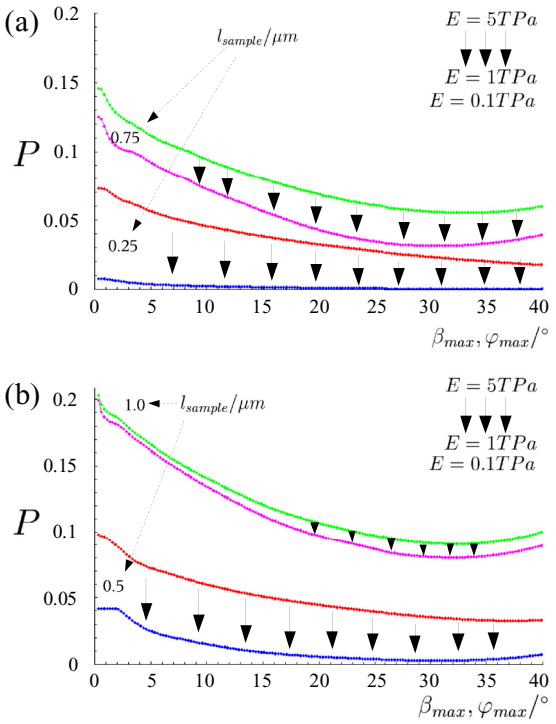

FIG. 12. (Color online) Mobile contact creation probability graphs for a distribution of full MWNTs (stiffest MWNTs possible) with parameters of Frank *et al.* [4]. The black arrows show how the probability decreases when $E = 5$ TPa is decreased to $E = 1$ TPa (or $E = 0.1$ TPa which gives the same calculation results). (a) $l_{\text{sample}} = 0.25\ \mu$m and $l_{\text{sample}} = 0.75\ \mu$m; (b) $l_{\text{sample}} = 0.5\ \mu$m and $l_{\text{sample}} = 1.0\ \mu$m.

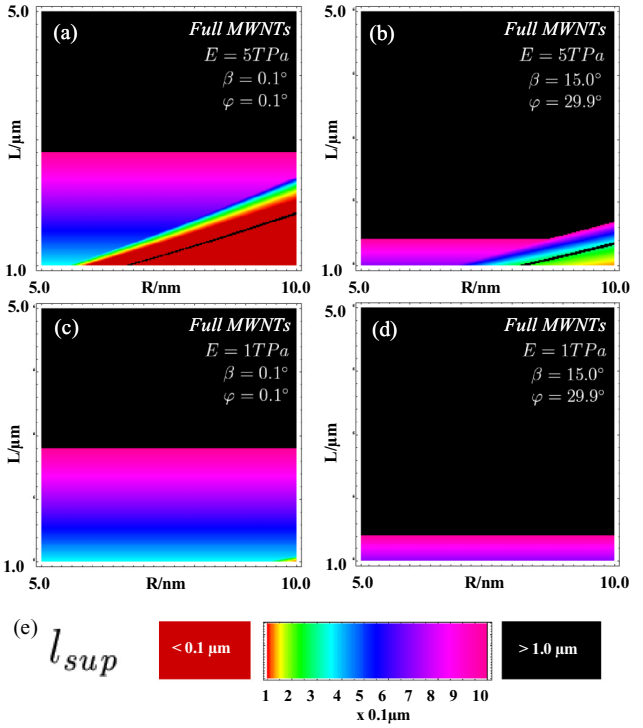

FIG. 13. (Color online) l_{sup} maps for a distribution of full MWNTs (stiffest MWNTs possible) with parameters of Kajiura *et al.* [10], (a) and (b) for $E = 5$ TPa; (c) and (d) for $E = 1$ TPa. ($\tau = 89.9^\circ$.)

with the liquid-metal contact method on this experimental CNT distribution cannot be interpreted in the simple way, even if we assume a high Young modulus $E = 5$ TPa for the CNTs.

If we perform the same simulation for the lower Young modulus of $E = 1$ TPa, the mobile contact creation probability drops even more. This change is brought out in Fig. 12. However, if the Young modulus is lowered any further, such as to $E = 0.1$ TPa, the mobile contact creation probability does almost not drop any further. Therefore, the results for both Young moduli $E = 1$ TPa and $E = 0.1$ TPa are shown in the same figure [Fig. 11(b)]. After what we learned above from the l_{sup} maps in Fig. 10, this is another strong indication that already for $E = 1$ TPa almost all CNTs creating a mobile contact are flexible; i.e., the mobile contact is only created through lying down on the Hg surface as no CNT of this distribution is rigid enough to penetrate the Hg surface. This means that the mobile creation probability, even if already very low, is still very likely to be highly overestimated.

For the experimental distribution of MWNTs of Kajiura *et al.* [10], the results are shown in Figs. 13, 14, and 15. Figure 13 shows some example l_{sup} maps for this distribution. The observations we can make from these maps are basically the same as from the maps corresponding to the MWNTs of Frank *et al.* [4] except for the fact that here the differential mobile contact creation probability is as high as 50% in the low-angle limit. However, this is only due to the flexible

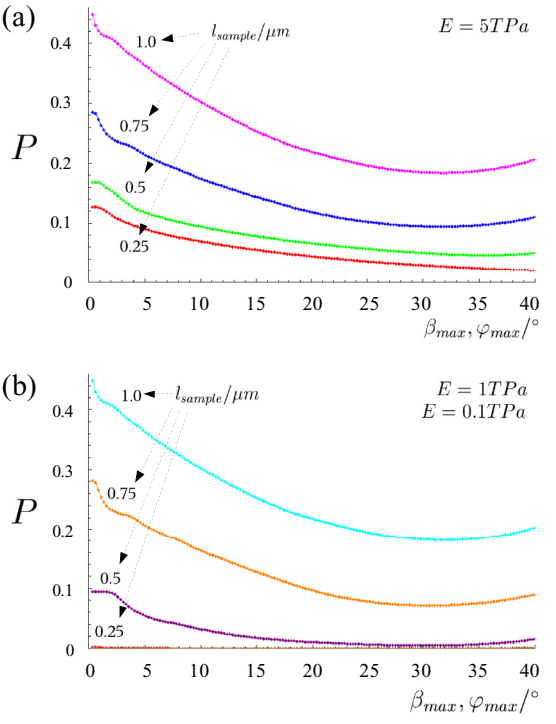

FIG. 14. (Color online) Mobile contact creation probability graphs for a distribution of full MWNTs (stiffest MWNTs possible) with parameters of Kajiura *et al.* [10], (a) for $E = 5$ TPa; (b) for $E = 1$ TPa and $E = 0.1$ TPa.

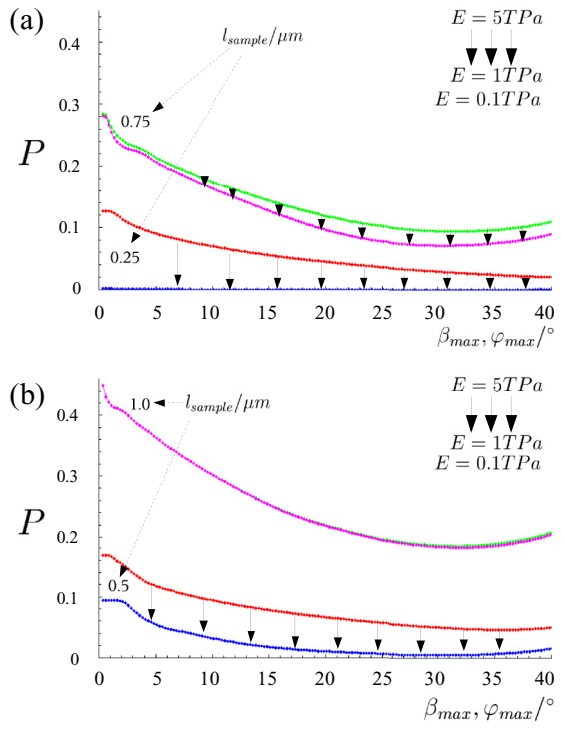

FIG. 15. (Color online) Mobile contact creation probability graphs for a distribution of full MWNTs (stiffest MWNTs possible) with parameters of Kajiura *et al.* [10]. The black arrows show how the probability decreases when $E = 5$ TPa is decreased to $E = 1$ TPa. (a) $l_{\text{sample}} = 0.25\ \mu$m and $l_{\text{sample}} = 0.75\ \mu$m; (b) $l_{\text{sample}} = 0.5\ \mu$m and $l_{\text{sample}} = 1.0\ \mu$m.

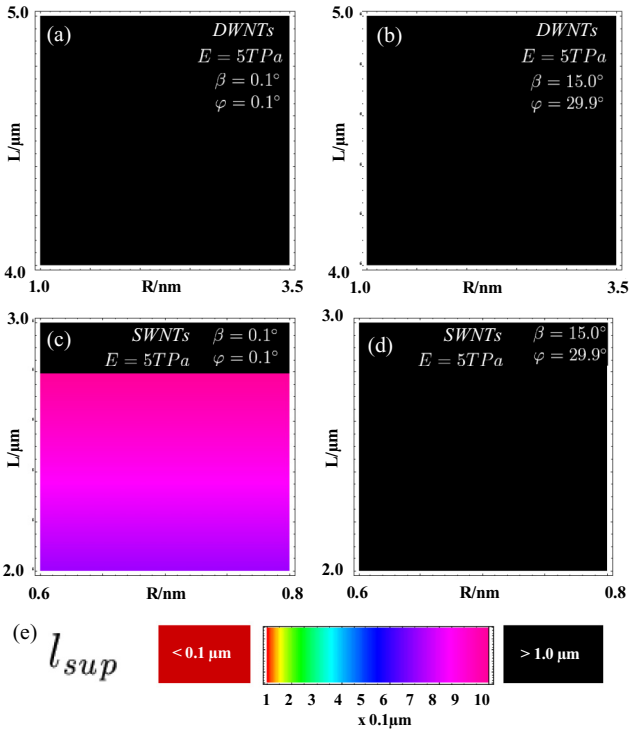

FIG. 16. (Color online) l_{sup} maps for (a) and (b) a distribution of DWNTs with parameters of Kajiura *et al.* [8]; (c) and (d) a distribution of SWNTs with parameters of Kajiura *et al.* [9]. ($E = 5$ TPa, $\tau = 89.9^\circ$.)

CNTs lying down on the Hg surface and therefore very likely overestimated.

Now, Fig. 14(a) tells us that for a typical experimentally achievable maximal misalignment angle of 30°, the probability of mobile contact creation is 2.9% for $l_{\text{sample}} = 0.25\ \mu$m, 5.0% for $l_{\text{sample}} = 0.5\ \mu$m, 9.5% for $l_{\text{sample}} = 0.75\ \mu$m, and 18.5% for $l_{\text{sample}} = 1.0\ \mu$m. We can conclude from these numbers that even if 18.5% of the CNTs created a mobile contact with the Hg after the sample has approached the Hg surface by 1.0 μm, still $18.5\% - 9.5\% = 9.0\%$ would have an error of at least 0.75 μm on the electronic mean-free path (EMFP) of the CNT one tries to determine by these experiments. Analogously, $9.5\% - 5.0\% = 4.5\%$ would have an error between 0.5 μm and 0.75 μm on the EMFP, $5.0\% - 2.9\% = 1.2\%$ an error between 0.25 μm and 0.5 μm on the EMFP, and 2.9% an error between 0 μm and 0.25 μm on the EMFP. Given the high proportion of flexible CNTs making a mobile contact with the Hg, these mobile contact creation probability values are very likely still noticeably overestimated. Therefore, transport experiments performed with the liquid-metal contact method on this experimental CNT distribution cannot be interpreted in the simple way, even if we assume a high Young modulus $E = 5$ TPa for the CNTs.

If we perform the same simulation for the lower Young modulus of $E = 1$ TPa, the mobile contact creation probability drops even more (except for $l_{\text{sample}} = 1\ \mu$m where the decrease of rigid CNTs creating a mobile contact is almost completely compensated by flexible CNTs creating a mobile contact). This change is brought out in Fig. 15. However, if the Young modulus is lowered any further, such as to $E = 0.1$ TPa, the mobile contact creation probability does not drop any further. Therefore, the results for both Young moduli $E = 1$ TPa and $E = 0.1$ TPa are shown in the same figure [Fig. 14(b)]. After what we learned above from the l_{sup} maps in Fig. 13, this is another strong indication that already for $E = 1$ TPa almost all CNTs creating a mobile contact are flexible; i.e., the mobile contact is only created through lying down on the Hg surface as no CNT of this distribution is rigid enough to penetrate the Hg surface. This means that the mobile creation probability, even if already very low, is still very likely to be highly overestimated.

For the experimental distribution of DWNTs of Kajiura *et al.* [8] and of SWNTs of Kajiura *et al.* [9], the results are shown in Figs. 16 and 17. Figures 16(a) and 16(b) show two example l_{sup} maps for the DWNT distribution. Both (a) the map for the low-angle limit and (b) the map for the midsize angles are completely black which strongly suggests that the mobile creation probability will be close to zero for this DWNT distribution.

Figures 16(c) and 16(d) show two example l_{sup} maps for the SWNT distribution. Here, the map for the midsize angles is completely black (meaning a zero differential mobile contact creation probability). In contrast, the map for the low-angle limit shows a differential mobile contact creation probability of 80%. However, this probability arises from flexible CNTs alone and is therefore very likely highly overestimated.

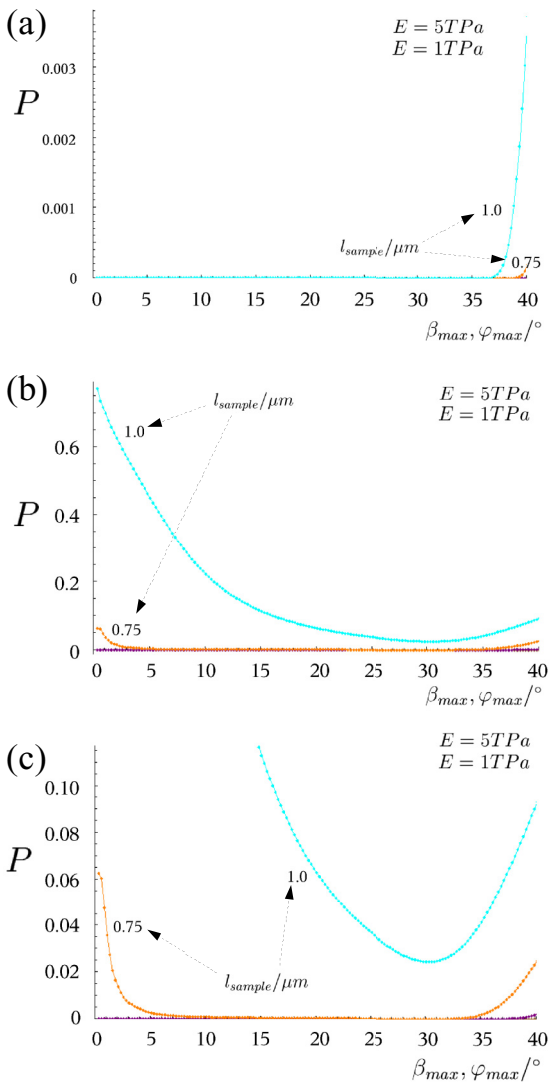

FIG. 17. (Color online) Mobile contact creation probability graphs for (a) a distribution of DWNTs with parameters of Kajiura *et al.* [8]; (b) and (c) a distribution of SWNTs with parameters of Kajiura *et al.* [9] ($E = 5$ TPa and $E = 1$ TPa).

It might appear surprising at first sight that the mobile creation probability is zero for this distribution of DWNTs and nonzero for this distribution of SWNTs even if DWNTs are more rigid than SWNTs. The explanation is simple: *Both* SWNTs and DWNTs from the here studied distributions are orders of magnitude below the rigidity which would be necessary in order to penetrate the Hg surface. (Hence, simulation results for $E = 5$ TPa and for $E = 1$ TPa are identical and are both represented in Fig. 17.) A mobile contact creation is therefore only possible through lying down on the Hg surface whereby the exact rigidity value of the CNT is irrelevant. The only here important parameter is the length of the CNT. Indeed, the here studied SWNTs are shorter than the DWNTs, and thus more likely to lie down on the Hg surface. However, we want to remind the reader that neither the lengths of the DWNTs nor the SWNTs have been clearly stated in respectively Kajiura *et al.* [8] or Kajiura *et al.* [9] and we have used our own estimations instead based on the figures from Kajiura *et al.* [8] and Kajiura *et al.* [9] (see Table I). This is another reason for which the here calculated mobile contact creation probability might be highly overestimated.

Indeed, Fig. 17 (a) confirms to us that the mobile contact creation probability for the here studied distribution of DWNTs of Kajiura *et al.* [8] is well below 1% for the whole angle range. This is a very clear result saying that the liquid-metal contact method cannot work for this DWNT distribution.

Figures 17(b) and 17(c) show us the simulation results for the SWNT distribution of Kajiura *et al.* [9]. Also here, we see that the mobile contact creation probability is zero over the whole angle range for the maximal sample displacements $l_{\text{sample}} = 0.25\ \mu$m and $l_{\text{sample}} = 0.5\ \mu$m. Also for $l_{\text{sample}} = 0.75\ \mu$m, the mobile contact creation probability stays below 1% except for very low angles ($<2.6^\circ$) and high angles ($> 37.6^\circ$). In contrast, for $l_{\text{sample}} = 1.0\ \mu$m, the mobile contact creation probability is above 50% for very low angles ($<4.35^\circ$) which however are experimentally unachievable. Instead, for a typical experimentally achievable maximal misalignment angle of 30°, the probability of mobile contact creation is only 2.4% for $l_{\text{sample}} = 1.0\ \mu$m. We can conclude from these numbers that even if 2.4% of the CNTs created a mobile contact with the Hg after the sample has approached the Hg surface by 1.0 μm, they all would have an error of at least 0.75 μm on the electronic mean free path (EMFP) of the CNT one tries to determine by these experiments. Given that only flexible SWNTs make a mobile contact with the Hg, these mobile contact creation probability values are very likely still highly overestimated. Therefore, transport experiments performed with the liquid-metal contact method on this experimental SWNT distribution cannot be interpreted in the simple way.

VII. CONCLUSION

In conclusion, our simulations of the mechanical interaction between the CNT and the Hg surface in liquid-metal contact (LMC) configuration show that most CNTs will not create a mobile contact with the Hg surface under realistic experimental conditions and that the apparent electronic mean-free path (EMFP) value deduced from LMC measurements will be exclusively due to elasticity induced CNT bending, geometry induced CNT sliding, and contact angle induced Hg meniscus related effects, and not to the electronic properties of the CNTs. In consequence, the LMC method is inapplicable for CNTs, in particular for CNTs with micrometric lengths which have been the focus of LMC experiments. Therefore, strong caution should be applied to the interpretation of LMC experiments claiming micrometric electronic mean free paths (EMFPs) in CNTs. These findings have strong consequences for the interpretation of previously reported works and we hope that they will help to resolve the controversy about the ballistic and diffusive nature of CNTs.

ACKNOWLEDGMENTS

The author thanks Professor Mathieu Kociak and Professor Christian Colliex for helpful comments and discussions on the physical modeling of the CNT-Hg interaction, the here presented results, and their presentation.

[1] S. Iijima, Nature (London) **354**, 56 (1991).

[2] R. Saito, G. Dresselhaus, and M. Dresselhaus, *Physical Properties of Carbon Nanotubes* (Imperial College Press, London, 1998).

[3] W. Hoenlein, G. S. Duesberg, A. P. Graham, F. Kreupl, M. Liebau, W. Pamler, R. Seidel, and E. Unger, Microelectron. Eng. **83**, 619 (2006).

[4] S. Frank, P. Poncharal, Z. L. Wang, and W. A. de Heer, Science **280**, 1744 (1998).

[5] A. Urbina, I. Echeverria, A. Perez-Garrido, A. Diaz-Sanchez, and J. Abellan, Phys. Rev. Lett. **90**, 106603 (2003).

[6] L. Langer, V. Bayot, E. Grivei, J. P. Issi, J. P. Heremans, C. H. Olk, L. Stockman, C. Van Haesendonck, and Y. Bruynseraede, Phys. Rev. Lett. **76**, 479 (1996).

[7] A. Bachtold, C. Strunk, J. P. Salvetat, J. M. Bonard, L. Forro, T. Nussbaumer, and C. Schonenberger, Nature (London) **397**, 673 (1999).

[8] H. Kajiura, H. J. Huang, and A. Bezryadin, Chem. Phys. Lett. **398**, 476 (2004).

[9] H. Kajiura, A. Nandyala, U. C. Coskun, A. Bezryadin, M. Shiraishi, and M. Ata, Appl. Phys. Lett. **86**, 122106 (2005).

[10] H. Kajiura, A. Nandyala, and A. Bezryadin, Carbon **43**, 1317 (2005).

[11] N. R. Wilson, D. H. Cobden, and J. V. Macpherson, J. Phys. Chem. B **106**, 13102 (2002).

[12] J. Y. Chen, A. Kutana, C. P. Collier, and K. P. Giapis, Science **310**, 1480 (2005).

[13] M. Kobylko, M. Kociak, Y. Sato, K. Urita, A. Bonnot, A. Kasumov, Y. Kasumov, K. Suenaga, and C. Colliex, Phys. Rev. B **90**, 195431 (2014).

[14] See Supplemental Material at http://link.aps.org/supplemental/10.1103/PhysRevB.90.195432 for the description of the physical modeling of the mechanical CNT-Hg interaction in the LMC method configuration.

[15] P.-G. de Gennes, F. Brochard-Wyart, and D. Quéré, *Gouttes, Bulles, Perles, et Ondes* (Belin, Paris, 2005).

[16] A. Awasthi, Y. J. Bhatt, and S. P. Garg, Meas. Sci. Technol. **7**, 753 (1996).

[17] E. Dujardin, T. W. Ebbesen, H. Hiura, and K. Tanigaki, Science **265**, 1850 (1994).

[18] E. Dujardin, T. W. Ebbesen, A. Krishnan, and M. M. J. Treacy, Adv. Mater. **10**, 1472 (1998).

[19] J. Israelachvili, *Intermolecular and Surfaces Forces* (Academic Press, Burlington, MA, 1991).

[20] R. C. Tolman, J. Chem. Phys. **17**, 333 (1949).

[21] R. C. Tolman, J. Chem. Phys. **16**, 758 (1948).

[22] R. C. Tolman, J. Chem. Phys. **17**, 118 (1949).

[23] A. E. van Giessen, E. M. Blokhuis, and D. J. Bukman, J. Chem. Phys. **108**, 1148 (1998).

[24] Y. A. Lei, T. Bykov, S. Yoo, and X. C. Zeng, J. Am. Chem. Soc. **127**, 15346 (2005).

[25] D. Schiff, Phys. Rev. **186**, 151 (1969).

[26] V. M. Samsonov, L. M. Shcherbakov, A. R. Novoselov, and A. V. Lebedev, Colloids Surf., A **160**, 117 (1999).

[27] H. M. Lu and Q. Jiang, Langmuir **21**, 779 (2005).

[28] B. I. Yakobson, C. J. Brabec, and J. Bernholc, Phys. Rev. Lett. **76**, 2511 (1996).

[29] J. P. Lu, Phys. Rev. Lett. **79**, 1297 (1997).

[30] E. Hernandez, C. Goze, P. Bernier, and A. Rubio, Phys. Rev. Lett. **80**, 4502 (1998).

[31] K. Enomoto, S. Kitakata, T. Yasuhara, N. Ohtake, T. Kuzumaki, and Y. Mitsuda, Appl. Phys. Lett. **88**, 153115 (2006).

[32] P. Poncharal, Z. L. Wang, D. Ugarte, and W. A. de Heer, Science **283**, 1513 (1999).

[33] I. Szabó, *Einführung in die Technische Mechanik* (Springer, Berlin, 2003).

[34] N. Grobert, Materials Today **10**, 28 (2007).

[35] Mathematica, Wolfram Research, http://www.wolfram.com.

[36] P. Poncharal, S. Frank, Z. L. Wang, and W. A. de Heer, Eur. Phys. J. D **9**, 77 (1999).

[37] Z. L. Wang, P. Poncharal, and W. A. de Heer, J. Phys. Chem. Solids **61**, 1025 (2000).

[38] P. Poncharal, C. Berger, Y. Yi, Z. L. Wang, and W. A. de Heer, J. Phys. Chem. B **106**, 12104 (2002).

[39] C. Berger, Y. Yi, J. Gezo, P. Poncharal, and W. A. de Heer, New J. Phys. **5**, 158 (2003).